THE JOURNAL OF PHYSICAL CHEMISTRY C

Article

pubs.acs.org/JPCC

Giant Magnetoresistive Phosphoric Acid Doped Polyaniline–Silica Nanocomposites

Hongbo Gu,[†,§] Jiang Guo,[†] Xi Zhang,[†,‡] Qingliang He,[†] Yudong Huang,[§] Henry A. Colorado,[∥] Neel Haldolaarachchige,[#] Huolin Xin,[⊥] David P. Young,[#] Suying Wei,*[,‡] and Zhanhu Guo*[,†]

[†]Integrated Composites Lab (ICL), Dan F. Smith Department of Chemical Engineering, Lamar University, Beaumont, Texas 77710, United States

[‡]Department of Chemistry and Biochemistry, Lamar University, Beaumont, Texas 77710, United States

[§]School of Chemical Engineering and Technology, Harbin Institute of Technology, Harbin 150001, Heilongjiang, China

[∥]Materials Science and Engineering, University of California, Los Angeles, California 90066, United States

[⊥]Materials Sciences Division, Lawrence Berkeley National Lab, Berkeley, California 94720, United States

[#]Department of Physics and Astronomy, Louisiana State University, Baton Rouge, Louisiana 70803, United States

Supporting Information

ABSTRACT: The phosphoric acid doped conductive polyaniline (PANI) polymer nanocomposites (PNCs) filled with silica nanoparticles (NPs) have been successfully synthesized using a facile surface initiated polymerization method. The chemical structures of the nanocomposites are characterized by Fourier transform infrared (FT-IR) spectroscopy. The enhanced thermal stability of the PNCs compared with that of pure PANI is observed by thermogravimetric analysis (TGA). The dielectric properties of these nanocomposites are strongly related to the silica nanoparticle loading levels. Temperature dependent resistivity analysis reveals a quasi 3-dimensional variable range hopping (VRH) electrical conduction mechanism for the synthesized nanocomposite samples. A positive giant magnetoresistance (GMR) is observed with a maximum value of 95.5% in the PNCs with a silica loading of 20.0 wt % and 65.6% for the pure PANI doped with phosphoric acid. The observed MR is well explained by wave function shrinkage model by calculating the changed localization length (ξ), density of states at the Fermi level ($N(E_F)$), and reduced average hopping length (R_{hop}). The effects of particle size on the properties including thermal stability, dielectric properties, temperature dependent resistivity, electrical conduction mechanism, and GMR of the nanocomposites are also studied.

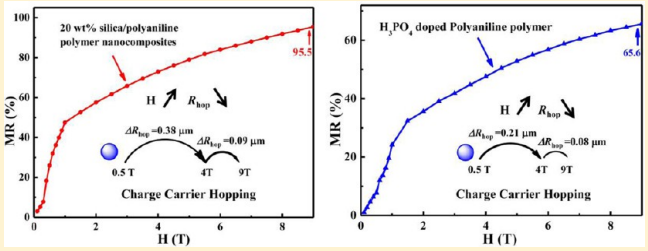

1. INTRODUCTION

Compared with traditional composites, conductive polymer nanocomposites (PNCs) have been deployed widely in areas including electronics,[1] sensors,[2] and electrocatalysts[3] due to their easy processability, flexibility,[4] and excellent electrical, optical, and magnetic properties.[5,6] Therefore, a great variety of multifunctional conductive PNCs have been prepared using layer-by-layer,[7] electrospinning,[8] electropolymerization,[9] and surface initiated polymerization techniques.[10,11] Among the conductive PNCs, significant efforts have been devoted to the polyaniline (PANI)-based PNCs due to their unique easy synthesis, controllable doping/dedoping process, and electrical and electrochemical properties.[12] As one of the most important conjugated polymers, PANI has many potential applications including sensors,[13] electrochemical mechanical actuators,[14] electrochromic supercapacitors,[15] and flexible electrodes.[16]

Silica (silicon dioxide, SiO_2), formed by the strong directional covalent bonds (Si–O, four oxygen atom array at the corner of a tetrahedron around a central silicon atom[17]), is one of the most commonly used substrates in many areas such as electronics manufacturing,[18] photodynamic therapy,[19] drug delivery,[20] bone regeneration,[21] catalysis,[22] and sensing[23] due to its unique properties including water solubility, chemical inertness, biocompatibility, and optical transparency.[24] Silica is often used to fabricate composites with high stability especially in harsh environments, including high temperatures and strong acids/bases.[25] Recently, there has been some research reported on the silica/PANI PNCs regarding the inkjet-printing electrochromic devices (doped with p-toluene sulfonic acid (PTSA) and synthesized by in situ polymerization),[26] conductive capsules and hollow spheres (doped with sulfonated polystyrene and synthesized by in situ polymerization),[27] and electrorheological responses (doped with dodecylbenzene sulfonic acid and synthesized by interfacial interaction).[28]

Received: November 20, 2012
Revised: February 22, 2013
Published: February 25, 2013

Since the first discovery of the giant magnetoresistance (GMR) effect in the thin-film structural metallic materials composed of a pair of ferromagnetic layers (Fe) separated by a nonmagnetic metal layer (Cr) in 1988,[29] GMR-based sensors have been designed and widely used in the areas including magnetic data storage (hard disc driver) and biological detection.[30] In the last few decades, carbon-based organic systems have been promising materials and have attracted more attention in the GMR effects, since the element carbon has weak spin−orbit coupling and hyperfine interaction.[31] Though the GMR in the organic systems has been obtained at low temperatures, the room temperature GMR signal is still too weak[32] and to obtain large GMR signal at room temperature is still a challenge. Recently, the GMR in the conductive polymers and their nanocomposites have been reported. For example, around 95 and 20% of GMR is observed in the 30 wt % Fe_3O_4/PANI nanocomposites[33] and 20 wt % $BaTiO_3$ (~500 nm)/PANI PNCs synthesized by the surface initiated polymerization method, and around 35% GMR is observed in the 20 wt % $BaTiO_3$ (~500 nm)/PANI PNCs prepared by a simple physical mixture of PANI and $BaTiO_3$ powders.[34] However, the GMR behaviors of the phosphoric acid (H_3PO_4) doped PANI and its silica PNCs together with the electrical conduction mechanism and dielectric properties have not been reported yet.

In this work, phosphoric acid doped conductive polyaniline nanocomposites filled with different silica nanoparticle loading levels and two different silica sizes have been successfully synthesized using a facile surface initiated polymerization (SIP) method. The chemical structures of the silica/PANI PNCs are characterized by Fourier transform infrared (FT-IR) spectroscopy. The thermal stability of the silica/PANI nanocomposites is performed by thermogravimetric analysis (TGA). Both scanning electron microscopy (SEM) and transmission electron microscopy (TEM) are used to characterize the morphologies of the silica/PANI nanocomposites. The temperature dependent resistivity and frequency dependent dielectric property are systematically investigated. The electrical conduction mechanism is studied from the temperature dependent resistivity analysis. The GMR properties in these nonmagnetic polymer and polymer nanocomposites are explained by the wave function shrinkage model by calculating the changed localization length (ξ), density of states ($N(E_F)$) at the Fermi level, and reduced average hopping length (R_{hop}). The particle size effects on the properties including thermal stability, dielectrical properties, temperature dependent resistivity, electrical conduction mechanism, and GMR behavior of these silica/PANI PNCs are investigated as well.

2. EXPERIMENTAL SECTION

2.1. Materials. Aniline (C_6H_7N) and ammonium persulfate (APS, $(NH_4)_2S_2O_8$) were purchased from Sigma Aldrich. Phosphoric acid (H_3PO_4, 85 wt %) was obtained from Fisher Scientific. The silica nanoparticles (NPs) with an average diameter of 60−70 nm (98+%, amorphous, specific surface area: 160−600 m^2/g) and 20−30 nm (99+%, amorphous, specific surface area: 180−600 m^2/g) were obtained from US Research Nanomaterials Inc. All of the chemicals were used as received without any further treatment.

2.2. Fabrication of Silica/PANI Nanocomposites. The silica/PANI nanocomposites were prepared with a surface initiated polymerization method. Briefly, the silica NPs (0.186−2.511 g), H_3PO_4 (15 mmol), and APS (9 mmol) were first added into 100 mL of deionized water in an ice−water bath for 1 h of mechanical stirring (SCILOGEX OS20-Pro LCD Digital Overhead Stirrer, 300 rpm) combined with sonication (Branson 8510). Then, the aniline solution (18 mmol in 25 mL of deionized water) was mixed with the above solution and mechanically stirred and sonicated continuously for an additional 1 h in an ice−water bath for further polymerization. The product was vacuum filtered and washed with deionized water. The precipitant was further washed with methanol to remove any possible oligomers. The final dark green silica/PANI nanocomposite powders were dried at 60 °C in an oven overnight. The silica (60−70 nm)/PANI nanocomposites with a particle loading of 10.0, 20.0, 40.0, and 60.0 wt % were synthesized, and the silica (20−30 nm)/PANI nanocomposites with a particle loading of 10.0 and 20.0 wt % were also synthesized to investigate the particle size effect on the properties of nanocomposites. Pure PANI doped with H_3PO_4 was also synthesized following the above same procedures without adding any NPs for comparison.

2.3. Characterizations. The Fourier transform infrared (FT-IR) spectra of the products were obtained on a Bruker Inc. Vector 22 (coupled with an ATR accessory) in the range 500−4000 cm^{-1} at a resolution of 4 cm^{-1}. The morphologies of the synthesized nanocomposites were observed on a field emission scanning electron microscope (SEM, JEOL, JSM-6700F system). The samples were prepared by adhering the powders onto an aluminum plate. Thermogravimetric analysis (TGA) was conducted by a TA Instruments TGA Q-500 instrument with a heating rate of 10 °C min^{-1} under an air flow rate of 60 mL min^{-1} from 30 to 800 °C.

Dielectric properties were investigated by an LCR meter (Agilent, E4980A) equipped with a dielectric test fixture (Agilent, 16451B) at a frequency of 20 to 2×10^6 Hz at room temperature. Pure PANI and its nanocomposite powders were pressed in a disc pellet form with a diameter of 25 mm by applying a pressure of 50 MPa in a hydraulic presser, and the average thickness was about 1.0 mm. The same sample was used to measure the resistivity (ρ) by a standard four-probe method from 180 to 290 K. The temperature dependent resistivity was used to determine the electrical conduction mechanism in the pure PANI and its nanocomposites.

Magnetoresistance (MR) was carried out using a standard four-probe technique by a 9-T Physical Properties Measurement System (PPMS) by Quantum Design at room temperature.

3. RESULTS AND DISCUSSION

3.1. FT-IR Analysis. Figure 1 shows the FT-IR spectra of the as-received silica NPs (60−70 nm), pure PANI doped with H_3PO_4, and its nanocomposites reinforced with different nanoparticle loadings. The strong absorption peaks at 1559 and 1474 cm^{-1} for the pure PANI doped with H_3PO_4, Figure 1f, correspond to the C═C stretching vibration of the quinoid and benzenoid rings, respectively.[35] The peak at 1290 cm^{-1} is related to the C—N stretching vibration of the benzenoid unit.[36] The peaks at 1239 and 1117 cm^{-1} are assigned to the C—H and C—N stretching vibrations of the quinoid rings, respectively.[33] The peak at around 785 cm^{-1} is attributed to the out-of-plane bending of C—H in the substituted benzenoid ring.[37] These peaks are in good agreement with previous FT-IR spectroscopic characterization of PANI[38] and have a little bit of shift (about 3−25 cm^{-1}) in the FT-IR spectra of the silica/PANI PNCs, Figure 1a−e, indicating a strong interaction between silica and PANI, which is related to the charge

dx.doi.org/10.1021/jp311471f | J. Phys. Chem. C 2013, 117, 6426−6436

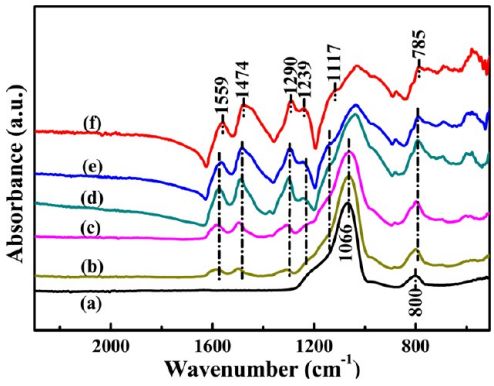

Figure 1. FT-IR spectra of (a) the as-received silica (60−70 nm); the silica (60−70 nm)/PANI PNCs with a nanoparticle loading of (b) 60.0, (c) 40.0, (d) 20.0, and (e) 10.0 wt %; and (f) pure PANI doped with H_3PO_4.

delocalization on the polymer backbone.[35] The absorption peaks at around 1066 and 800 cm^{-1} are attributed to the stretching and bending vibrations of Si−O bonding,[39] respectively, Figure 1a, and the peak intensity at around 1066 cm^{-1} increases with increasing silica nanoparticle loading in the silica/PANI PNCs, Figure 1b−d.

3.2. Thermogravimetric Analysis. Figure 2 shows the TGA curves of the as-received silica NPs (60−70 nm), pure

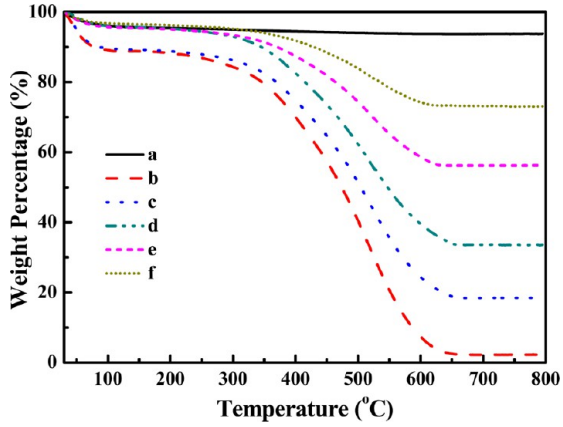

Figure 2. TGA curves of (a) the as-received silica (60−70 nm) nanoparticles; (b) pure PANI doped with H_3PO_4; and the silica (60−70 nm)/PANI PNCs with a nanoparticle loading of (c) 10.0, (d) 20.0, (e) 40.0, and (f) 60.0 wt %.

PANI doped with H_3PO_4 and its nanocomposites with different silica nanoparticle loadings in the air. For the as-received silica nanoparticles, there is only a slight weight loss (6.1 wt %) around 150 °C during the measured temperature range from 30 to 800 °C due to the loss of moisture. Two-stage weight losses are observed in the pure PANI and its nanocomposites. The first stage in the temperature range from room temperature to 250 °C is due to the elimination of moisture and the doped H_3PO_4 in PANI.[34] The major weight loss of all the samples from 250 to 600 °C is due to the large scale thermal degradation of the PANI chains.[40] Table 1 shows the summarized thermal properties of pure PANI doped with H_3PO_4 and its nanocomposites. The thermal stability of the silica/PANI PNCs is observed to increase with increasing silica nanoparticle loading. The 15 wt % loss decomposition temperature for pure PANI doped with H_3PO_4 and its PNCs

Table 1. Thermal Stability of the H_3PO_4 Doped PANI and Its Silica Nanocomposites

samples	15.0 wt % loss decomposition temperature (°C)	weight residue at 800 °C (wt %)
H_3PO_4 doped PANI	288	2.11
silica (60−70 nm)/PANI PNCs		
10.0 wt %	321	18.48
20.0 wt %	384	33.54
40.0 wt %	423	56.34
60.0 wt %	489	73.06
silica (20−30 nm)/PANI PNCs		
10.0 wt %	300	17.31
20.0 wt %	357	32.36

with a silica nanoparticle loading of 10.0, 20.0, 40.0, and 60.0 wt % is 288, 321, 384, 423, and 489 °C, respectively. This increased thermal stability is attributed to the strong interaction between PANI and silica NPs and the lower mobility of the polymer chains when the polymer is bounded on the surface of silica NPs.[41] In addition, the thermal stability of the H_3PO_4 doped PANI is lower than that of the p-toluene sulfonic acid (PTSA) doped PANI due to the presence of the benzene ring in the PTSA chemical structure (the 15 wt % loss decomposition temperature for the former is 288 and 303 °C for the latter[33]). The pure PANI is almost completely decomposed at 800 °C with only 2.11 wt % left, which is due to the carbonized PANI. The weight residues of the nanocomposites with an initial silica nanoparticle loading of 10.0, 20.0, 40.0, and 60.0 wt % at 800 °C are 18.48, 33.54, 56.34, and 73.06%, respectively. The difference in the weight residues from the initially calculated particle loading based on the monomers and particles is associated with the incomplete polymerization of the aniline monomers.[33]

3.3. Microstructures of the Nanocomposites. Figure 3 shows the SEM microstructures of the as-received silica nanoparticles (60−70 nm), pure PANI doped with H_3PO_4, and its PNCs. The PANI doped with H_3PO_4 is observed to have a rough and flake-like surface, Figure 3A. However, the as-received silica nanoparticles have a fairly smooth and ball-like surface, Figure 3B. These obvious differences on the surface are used to distinguish PANI from silica nanoparticles. In the PNCs, the smooth and ball-like surface of the silica nanoparticles is observed to become rough and flake-like, Figure 3C, indicating the polymerization of PANI occurred on the silica nanoparticle surface.[36]

3.4. Dielectric Properties. The dielectric properties of the PNCs are related to the charge carrier motion within the matrix[11] and interfacial polarization between the hosting polymer matrix and the nanofillers.[42] Figure 4 depicts the real permittivity (ε', Figure 4A), imaginary permittivity (ε'', Figure 4B), and dielectric loss ($\tan\delta$, where $\tan\delta = \varepsilon''/\varepsilon'$, Figure 4C) as a function of frequency for the pure PANI doped with H_3PO_4 and its PNCs with different silica (60−70 nm) loadings within the frequency range from 20 to 2×10^6 Hz at room temperature. In Figure 4A, all the samples exhibit positive ε' within the measured frequency range and have an extremely high value at low frequency (20 Hz), then the ε' decreases sharply with increasing frequency at low frequency range (<110 Hz), and it finally slightly decreases with further increase of the frequency. Compared with the PTSA doped PANI (negative

dx.doi.org/10.1021/jp311471f | J. Phys. Chem. C 2013, 117, 6426−6436

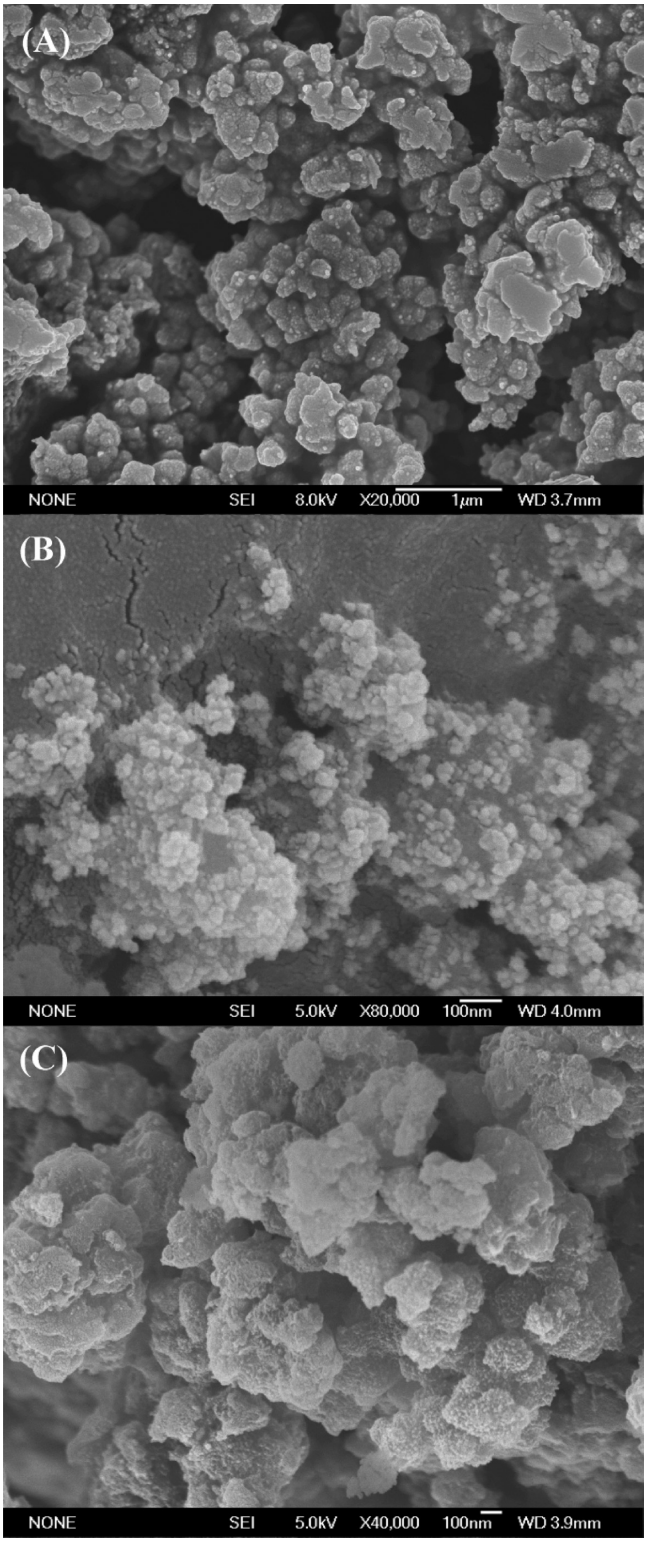

Figure 3. SEM microstructures of (A) pure PANI doped with H_3PO_4; (B) the as-received silica nanoparticles (60−70 nm); and (C) the silica (60−70 nm)/PANI PNCs with a nanoparticle loading of 20.0 wt %.

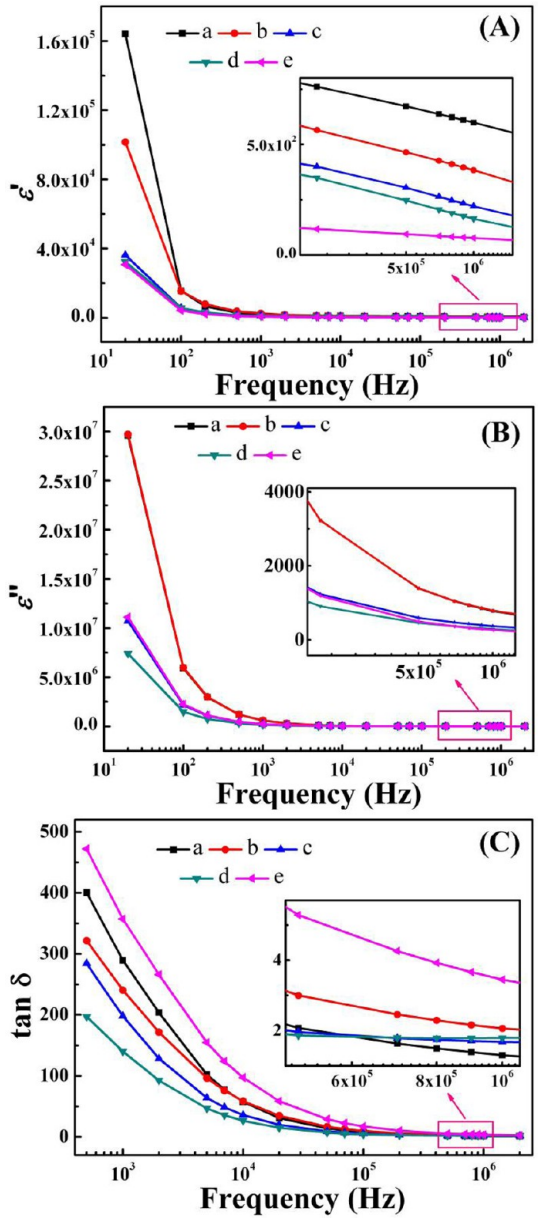

Figure 4. (A) Real permittivity, (B) imaginary permittivity, and (C) dielectric loss as a function of frequency of (a) pure PANI doped with H_3PO_4 and the silica (60−70 nm)/PANI PNCs with a nanoparticle loading of (b) 10.0, (c) 20.0, (d) 40.0, and (e) 60.0 wt %.

permittivity from −32 to −12 within the whole measured frequency range from 20 to 2 × 10^6 Hz),[33] the H_3PO_4 doped PANI shows a huge positive ε' with order of 10^5 at a frequency of 20 Hz. The large positive permittivity of PANI represents charge delocalization that occurs in the mesoscopic range.[43] The ε' of the silica/PANI nanocomposites is found to decrease with increasing silica nanoparticle loading. For the low loading of silica/PANI PNCs, the large ε' is mainly attributed to the interfacial polarization, where the charge carriers are accumulated at the internal interfaces originated from the Maxwell−Wagner−Sillars polarization effect.[44] However, for the nanocomposites with high silica nanoparticle loading, the ε' decreases dramatically owing to the low dielectric constant (≈1.8−2.5) of silica[45] compared with the H_3PO_4 doped PANI matrix. The ε'' is observed to have the same trend as ε' and decreases as the frequency increases to 10^2 Hz and then slightly decreases with increasing frequency to 10^6 Hz. The tan δ is also observed to have the same trend as ε' and ε''. In the high frequency range (10^5−10^6 Hz), tan δ has a very small value and almost reaches zero, indicating that these nanocomposites can be used as electronic devices with less energy waste.[35] The significantly higher tan δ of the silica/PANI PNCs with a silica

dx.doi.org/10.1021/jp311471f | J. Phys. Chem. C 2013, 117, 6426−6436

nanoparticle loading of 60 wt % compared with other loadings within the whole frequency range is attributed to the completely constructed charge transport channel.[11]

3.5. Temperature Dependent Resistivity - Electrical Conduction Mechanism. The temperature dependent resistivity of the H_3PO_4 doped PANI and its nanocomposites with different silica nanoparticle loadings is measured from 180 to 290 K, Figure 5A. Normally, the electrical conductivity of the

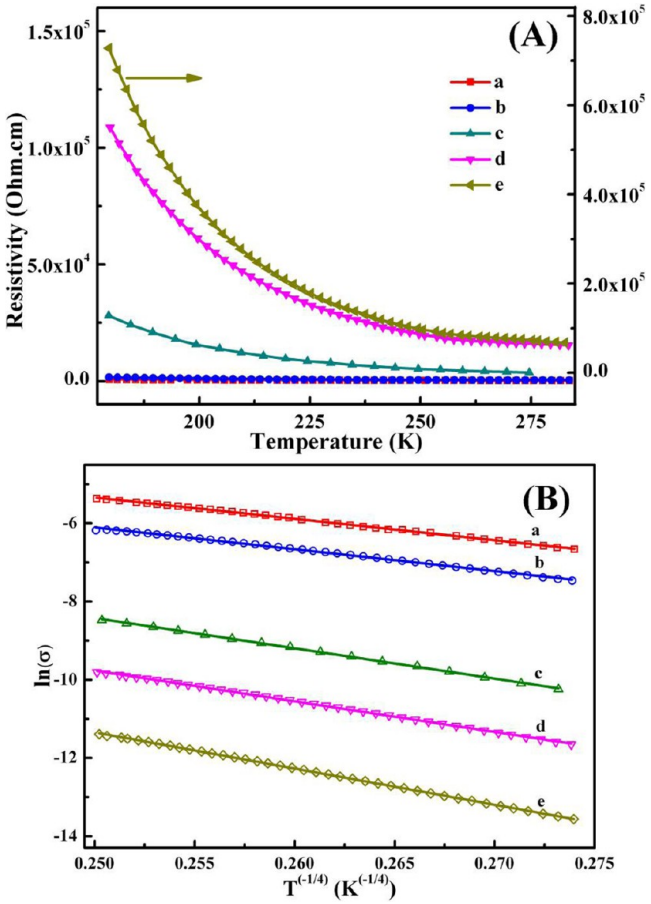

Figure 5. (A) Resistivity vs temperature and (B) $\ln(\sigma)$ and $T^{-1/4}$ curve of (a) pure PANI doped with H_3PO_4 and the silica (60–70 nm)/PANI PNCs with a nanoparticle loading of (b) 10.0, (c) 20.0, (d) 40.0, and (e) 60.0 wt %.

acid doped PANI strongly depends on the doped acid with electron donor ability[46] and is about 8–11 orders of magnitude (10^{-1}–10^{2} S cm^{-1})[47] higher than that of the PANI base (10^{-9} S·cm^{-1}).[48] In Figure 5A, all of the prepared samples exhibit a semiconductive behavior within the measured temperature range and the resistivity decreases with increasing temperature.[49] The resistivity of the H_3PO_4 doped PANI (1.7×10^3 and 4.6×10^2 Ω·cm for 180 K and room temperature, respectively) is higher than that of the PTSA doped PANI (6.0×10^2 and 2.0×10^2 Ω·cm for 180 K and room temperature, respectively).[33] The resistivity increases with increasing silica nanoparticle loading, since the silica nanoparticles affect the interaction between the PANI polymer matrix and the doped acid, which partially blocks the charge transport pathway.[50]

The electrical conduction mechanism is explored by the Mott variable range hopping (VRH) approach,[51] represented as eq 1:

$$\sigma = \sigma_0 \exp\left[-\left(\frac{T_0}{T}\right)^{1/(n+1)}\right] \quad (1)$$

where σ_0 is a constant, standing for the conductivity at infinitely low temperature, T is the Kelvin temperature, and the constant T_0 (K) is the characteristic Mott temperature, which relates to the energy needed for the charge carrier's hopping and given by eq 2:[52]

$$T_0 = 24/[\pi k_B N(E_F)\xi^3] \quad (2)$$

where ξ (nm) is the localization length of the localized wave function of charge carriers, k_B is Boltzmann's constant, and $N(E_F)$ ((J cm^3)$^{-1}$, (J = kg m^2 s^{-2})) is the density of states at the Fermi level. Equation 2 indicates that T_0 is related to both the density of states at the Fermi level $N(E_F)$ and the localization length ξ. The n value in eq 1 is related to the dimensionality of the conduction process and n = 3, 2, and 1 for the 3-, 2-, and 1-dimensional systems, respectively.[53] σ_0 and T_0 can be obtained from the intercept and the slope of the plot $\ln(\sigma) \sim T^{-1/(n+1)}$. The plot of $\ln(\sigma) \sim T^{-1/(n+1)}$ (obtained from Figure 5A) is shown in Figure 5B. The temperature dependent resistivity of pure PANI doped with H_3PO_4 and its nanocomposites with different silica nanoparticle loadings is observed to follow a $\ln(\sigma) \sim T^{-1/4}$ linear relationship, indicating a quasi 3-d VRH electrical conduction mechanism. The obtained σ_0 and T_0 values from Figure 5B are summarized in Table 2. Both T_0 and σ_0 of the H_3PO_4 doped PANI ($(9.48 \pm 0.23) \times 10^6$ K and 5319.289 ± 0.010 S cm^{-1}, respectively) are higher than those of the PTSA doped PANI (7.0×10^6 K and 1826 S cm^{-1}, respectively).[33] T_0 is reported to be strongly dependent on the disorder (which represents random potential fluctuation in the semiconductor;[54] in PANI, the disorder means the sequence of quinoid–benzenoid groups is random[55]) presented in the samples and can be measured by the resistivity ratio (ρ_r, $\rho_r = \rho_{180}/\rho_{290}$).[56] Generally, both the disorder in the samples and T_0

Table 2. T_0, σ_0, and ρ_r for the H_3PO_4 Doped PANI and Its Silica Nanocomposites

samples	$T_0 \times 10^7$ (K)	σ_0 (S cm^{-1})	ρ_r
H_3PO_4 doped PANI	0.948 ± 0.023	5319.289 ± 0.010	3.641
silica (60–70 nm)/PANI			
10.0 wt %	1.146 ± 0.017	4812.057 ± 0.007	4.358
20.0 wt %	3.217 ± 0.121	32039.987 ± 0.018	5.291
40.0 wt %	4.166 ± 0.033	32112.192 ± 0.004	7.087
60.0 wt %	5.784 ± 0.266	32130.789 ± 0.025	10.801
silica (20–30 nm)/PANI			
10.0 wt %	1.157 ± 0.006	4998.984 ± 0.009	3.742
20.0 wt %	2.022 ± 0.072	8440.949 ± 0.017	5.031

dx.doi.org/10.1021/jp311471f | J. Phys. Chem. C 2013, 117, 6426–6436

increase with increasing ρ_r.[57] In the silica/PANI nanocomposite system, the calculated ρ_r is listed in Table 2. ρ_r increases with increasing silica nanoparticle loading, indicating that the disorder in the silica/PANI nanocomposites increases with increasing silica nanoparticle loading. T_0 of the silica/PANI nanocomposites is also found to increase with increasing silica nanoparticle loading, indicating a larger number of defects and increased ρ_r.[58] Normally, the defects (e.g., dopants or impurities) can perturb the electronic structure of the semiconductors and act as scattering centers for charge carriers and holes traveling through the semiconductors to affect the charge carrier transport in the semiconductors[59] Thus, the observed larger T_0 is attributed to the stronger charge carrier scattering, Table 2. The σ_0 slightly decreases as the silica nanoparticle loading increases to 10.0 wt % and then increases obviously with increasing silica nanoparticle loading to 20.0 wt %. After that, the σ_0 slightly increases with increasing silica nanoparticle loading. A bigger T_0 corresponds to a higher σ_0, which is due to the modulated electromagnetic wave[33] (the electromagnetic wave propagating in a semiconductor along the direction of an alternating magnetic field becomes modulated at the frequency of electrical field[60]) in the nanostructures of the silica/PANI nanocomposites.

3.6. Magnetoresistance (MR). The magnetoresistance (MR) is defined by eq 3:

$$\mathrm{MR}\% = \frac{\Delta R}{R} = \frac{R(H) - R(0)}{R(0)} \times 100 \tag{3}$$

where $R(0)$ and $R(H)$ are the resistance at zero magnetic field and at any applied magnetic field H, respectively. The MR results of the H_3PO_4 doped PANI and its nanocomposites with different silica nanoparticle loadings at 290 K are shown in Figure 6. The MR for all of the samples is observed to be

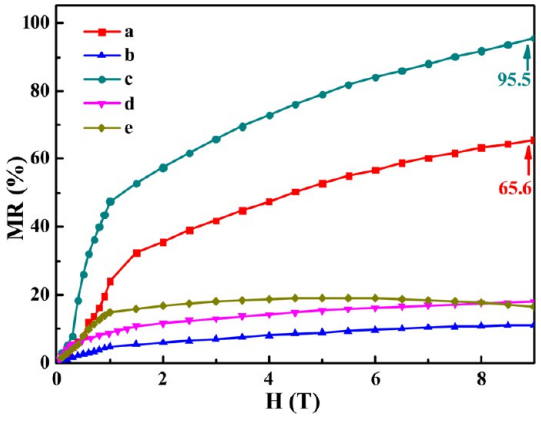

Figure 6. Magnetoresistance of (a) pure PANI doped with H_3PO_4 and the silica (60−70 nm)/PANI PNCs with a nanoparticle loading of (b) 10.0, (c) 20.0, (d) 40.0, and (e) 60.0 wt % at 290 K.

positive within the whole measured magnetic field and increases with increasing applied magnetic field and then reaches the maximum value at high field. The MR of the H_3PO_4 doped PANI (65.6%) is found to be higher than that of the PTSA doped PANI (53%).[33] The MR value of the silica/PANI nanocomposites increases as the silica nanoparticle loading increases to 20.0 wt % (95.5%) (MR is 11.5% for 10.0 wt % silica/PANI nanocomposiets) and then decreases with increasing silica nanoparticle loading. The MR values of the silica/PANI nanocomposites with a silica nanoparticle loading of 40.0 and 60.0 wt % are almost the same (around 17%) at a high applied magnetic field of 9 T. The slope of MR curves at low magnetic field indicates the MR sensitivity of the materials to an applied magnetic field.[61] The slope of MR curves for the H_3PO_4 doped PANI and its silica/PANI nanocomposites with a nanoparticle loading of 10.0, 20.0, 40.0, and 60.0 wt % is 0.0017, 0.0005, 0.0073, 0.0018, and 0.0015, respectively, indicating that the MR sensitivity obeys the following relationship: 10.0 wt % silica/PANI PNCs < 60.0 wt % silica/PANI PNCs < H_3PO_4 doped PANI < 40.0 wt % silica/PANI PNCs < 20.0 wt % silica/PANI PNCs. These materials with high MR sensitivity to the external magnetic field could be used as magnetic field sensors.[62]

The wave function shrinkage model is often used to describe the MR of highly disorderedly localized systems in the variable-range hopping (VRH) regime.[63] In this model, the contraction of the electronic wave function at impurity centers under a magnetic field leads to a reduction in the hopping probability between two sites, which causes a positive MR. In this model, the ratio of $R(H, T)$ and $R(0, T)$ is described as eq 4:[63]

$$R(H, T)/R(0, T) = \exp\{\zeta_C(0)[\zeta_C(H)/\zeta_C(0) - 1]\} \tag{4}$$

where $\zeta_C(0) = (T_0/T)^{1/4}$ for the Mott VRH conduction mechanism and $\zeta_C(H)/\zeta_C(0)$ is the normalized hopping probability parameter and is a function of H/P_C for the Mott VRH conduction mechanism. H is the magnetic field (Tesla, unit of magnetic field, 1 T = 10^4 Oe, T = kg C^{-1} s^{-1}), and P_C is the fitting parameter given by eq 5 for the Mott VRH conduction mechanism:

$$P_C = 6\hbar/[e\xi^2(T_0/T)^{1/4}] \tag{5}$$

where e is the electron charge ($1.6021765 \times 10^{-19}$ C), $\hbar$ is the reduced Planck's constant and $\hbar = h/2\pi$, h is Planck's constant, and T_0 is the Mott characteristic temperature (K). In the low-field limit, eq 4 is simplified to eq 6:

$$R(H, T)/R(0, T) \approx 1 + t_2\frac{H^2}{P_C^2}\left(\frac{T_0}{T}\right)^{1/4} \tag{6}$$

And the MR is defined in eq 7:

$$\begin{aligned}\mathrm{MR} &= \frac{R(H, T) - R(0, T)}{R(0, T)} \\ &\approx t_2\frac{H^2}{P_C^2}\left(\frac{T_0}{T}\right)^{1/4} \\ &= t_2\frac{e^2\xi^4}{36\hbar^2}\left(\frac{T_0}{T}\right)^{3/4}H^2\end{aligned} \tag{7}$$

where the numerical constant is $t_2 = 5/2016$.[64]

According to eq 7, the localization length ξ could be obtained by eq 8 from T_0, MR value, and magnetic field H:

$$\xi^4 = \frac{36\hbar^2\mathrm{MR}}{t_2e^2}\left(\frac{T_0}{T}\right)^{-3/4}H^{-2} \tag{8}$$

For example, T_0 is $(9.48 \pm 0.23) \times 10^6$ K for the H_3PO_4 doped PANI, and the calculated ξ from eq 8 for temperature at T = 290 K is 94.3 ± 2.3, 52.5 ± 1.3, and 37.6 ± 0.9 nm for a magnetic field H of 0.5, 4, and 9 T. The calculated localization length ξ of the silica/PANI nanocomposites with different silica loadings is shown in Table 3. ξ has different values under

dx.doi.org/10.1021/jp311471f | J. Phys. Chem. C 2013, 117, 6426−6436

Table 3. ξ, $N(E_F)$, R_{hop}, and ΔR_{hop} for the H_3PO_4 Doped PANI and Its Silica Nanocomposites at Different Magnetic Fields H

samples	parameters	magnetic field H (T) 0.5	4	9
H_3PO_4 doped PANI	ξ (nm)	94.3 ± 2.3	52.5 ± 1.3	37.6 ± 0.9
	$N(E_F)$ (J cm^3)$^{-1}$	(6.9 ± 0.5) × 10^{31}	(4.0 ± 0.3) × 10^{32}	(1.1 ± 0.1) × 10^{33}
	R_{hop} (μm)	0.475 ± 0.012	0.264 ± 0.007	0.190 ± 0.005
	ΔR_{hop} (μm)	(0.5 → 4 T) = 0.211 ± 0.014, (0.5 → 9 T) = 0.285 ± 0.013, (4 → 9 T) = 0.074 ± 0.009		
silica (60−70 nm)/PANI PNCs				
10.0 wt %	ξ (nm)	68.8 ± 1.0	32.6 ± 0.5	23.6 ± 0.4
	$N(E_F)$ (J cm^3)$^{-1}$	(1.5 ± 0.1) × 10^{32}	(1.4 ± 0.1) × 10^{33}	(3.7 ± 0.2) × 10^{33}
	R_{hop} (μm)	0.363 ± 0.005	0.172 ± 0.002	0.124 ± 0.002
	ΔR_{hop} (μm)	(0.5 → 4 T) = 0.191 ± 0.005, (0.5→ 9 T) = 0.239 ± 0.005, (4 → 9 T) = 0.048 ± 0.003		
20.0 wt %	ξ (nm)	101.8 ± 3.8	46.6 ± 1.8	33.2 ± 1.2
	$N(E_F)$ (J cm^3)$^{-1}$	(1.6 ± 0.1) × 10^{31}	(1.7 ± 0.2) × 10^{32}	(4.7 ± 0.5) × 10^{32}
	R_{hop} (μm)	0.697 ± 0.027	0.319 ± 0.013	0.227 ± 0.009
	ΔR_{hop} (μm)	(0.5 → 4 T) = 0.378 ± 0.030, (0.5 → 9 T) = 0.470 ± 0.016, (4 → 9 T) = 0.092 ± 0.016		
40.0 wt %	ξ (nm)	68.6 ± 0.5	29.5 ± 0.2	20.9 ± 0.2
	$N(E_F)$ (J cm^3)$^{-1}$	(4.1 ± 0.1) × 10^{31}	(5.2 ± 0.1) × 10^{32}	(1.5 ± 0.1) × 10^{33}
	R_{hop} (μm)	0.501 ± 0.004	0.215 ± 0.008	0.153 ± 0.004
	ΔR_{hop} (μm)	(0.5 → 4 T) = 0.286 ± 0.009, (0.5 → 9 T) = 0.348 ± 0.006, (4 → 9 T) = 0.062 ± 0.009		
60.0 wt %	ξ (nm)	67.8 ± 3.1	29.7 ± 1.4	19.2 ± 0.9
	$N(E_F)$ (J cm^3)$^{-1}$	(3.1 ± 0.3) × 10^{31}	(3.7 ± 0.5) × 10^{32}	(1.4 ± 0.2) × 10^{33}
	R_{hop} (μm)	0.537 ± 0.025	0.235 ± 0.011	0.152 ± 0.007
	ΔR_{hop} (μm)	(0.5 → 4 T) = 0.302 ± 0.027, (0.5 → 9 T) = 0.385 ± 0.026, (4 → 9 T) = 0.083 ± 0.013		
silica (20−30 nm)/PANI PNCs				
10.0 wt %	ξ (nm)	68.6 ± 0.4	32.5 ± 0.2	23.5 ± 0.1
	$N(E_F)$ (J cm^3)$^{-1}$	(1.5 ± 0.1) × 10^{32}	(1.4 ± 0.1) × 10^{33}	(3.7 ± 0.1) × 10^{33}
	R_{hop} (μm)	0.363 ± 0.002	0.172 ± 0.001	0.125 ± 0.001
	ΔR_{hop} (μm)	(0.5 → 4 T) = 0.191 ± 0.002, (0.5 → 9 T) = 0.238 ± 0.002, (4 → 9 T) = 0.047 ± 0.001		
20.0 wt %	ξ (nm)	111.2 ± 4.0	50.6 ± 1.8	36.1 ± 1.3
	$N(E_F)$ (J cm^3)$^{-1}$	(1.9 ± 0.2) × 10^{31}	(2.1 ± 0.2) × 10^{32}	(5.7 ± 0.6) × 10^{32}
	R_{hop} (μm)	0.678 ± 0.025	0.308 ± 0.011	0.220 ± 0.008
	ΔR_{hop} (μm)	(0.5 → 4 T) = 0.370 ± 0.027, (0.5 → 9 T) = 0.458 ± 0.026, (4 → 9 T) = 0.088 ± 0.014		

dx.doi.org/10.1021/jp311471f | J. Phys. Chem. C 2013, 117, 6426−6436

Scheme 1. Proposed GMR Mechanism in Silica/PANI Nanocomposites

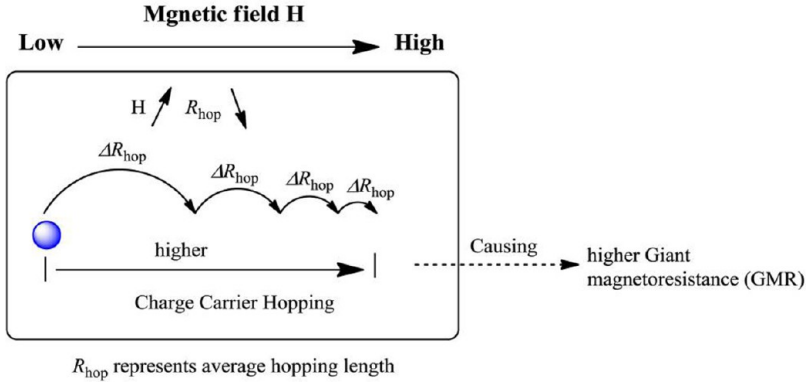

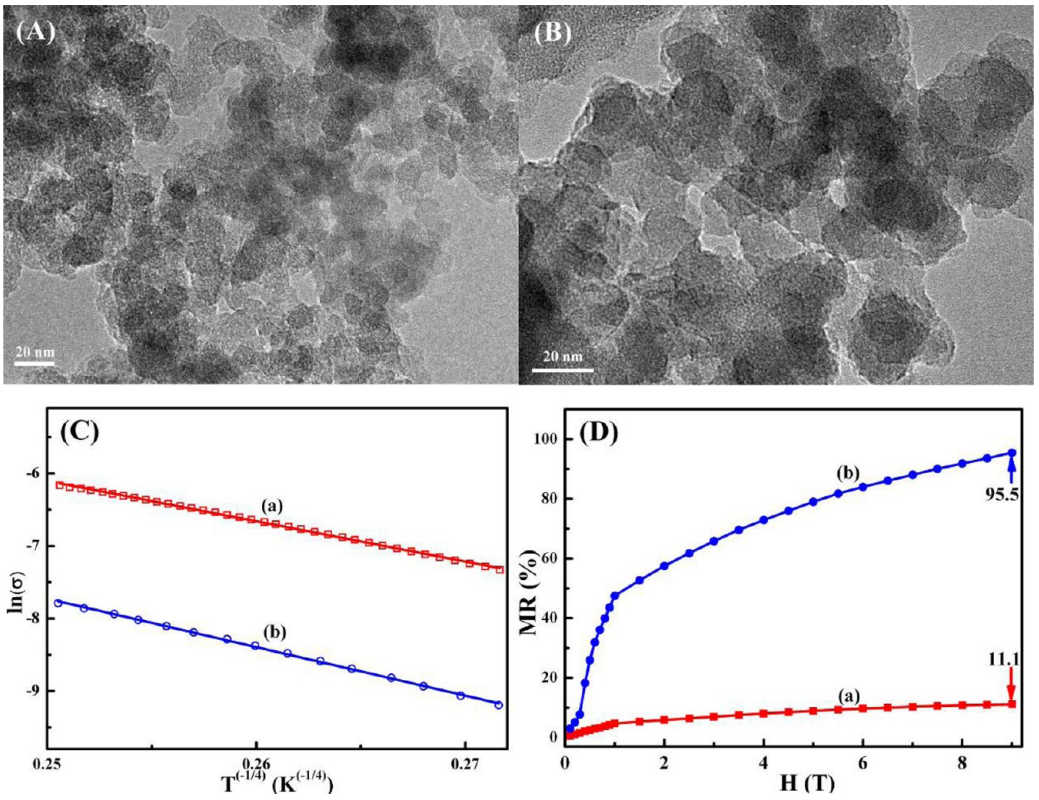

Figure 7. TEM microstructures of (A) the as-received small silica nanoparticles (20−30 nm), (B) the silica (20−30 nm)/PANI PNCs with a particle loading of 20.0 wt %; (C) the ln(σ) and $T^{-1/4}$ curve of silica (20−30 nm)/PANI PNCs with a particle loading of (a) 10.0 and (b) 20.0 wt %; (D) room temperature MR of the silica (20−30 nm)/PANI PNCs with a particle loading of (a) 10.0 and (b) 20.0 wt %.

different magnetic fields. After ξ was obtained, the density of states at the Fermi level $N(E_F)$ could be calculated from eq 9:

$$N(E_F) = 24/[\pi k_B T_0 \xi^3] \quad (9)$$

and the calculated results are listed in Table 3. Generally, the increased $N(E_F)$ could increase the hopping probability between the localized states.[65]

According to Entin-Wohlman et al.,[66] the MR value in the small magnetic fields should be proportional to the square of the flux (AH, where A is the area and H is the magnetic field) inside a coherent threading loop and can be described by eq 10:

$$\mathrm{MR} = \Delta R/R \sim A^2H^2 = R_{hop}{}^3(T, c, H)a(c, H)H^2 \quad (10)$$

where R_{hop} is the average hopping length, a is the microscopic length (i.e., the typical distance between impurities[67]), and c is the carrier concentration. For a given sample under small magnetic fields, both R_{hop} and a are at the weakest functions of the field and thus MR is only related to T and H and can be simplified to eq 11:[68]

$$\mathrm{MR} = \Delta R/R = f(T)H^2 \sim R_{hop}{}^3H^2 \quad (11)$$

This equation confirms that the MR value is also related to the average hopping length R_{hop}. The average hopping length could be calculated by eq 12 from the localization length ξ:

$$R_{hop} = (3/8)(T_0/T)^{1/4}\xi \quad (12)$$

The calculated R_{hop} (μm) values are shown in Table 3, and the results show that, in the silica/PANI PNCs, the more reduced R_{hop} (ΔR_{hop}), the higher value of MR obtained. Normally, the MR in the hopping system is due to the charge carrier hopping

dx.doi.org/10.1021/jp311471f | J. Phys. Chem. C 2013, 117, 6426−6436

conduction arising from the contraction of the charge carrier wave function and the subsequent reduced average hopping length.[11] Our results in the silica/PANI nanocomposite systems further confirm this conclusion. The proposed GMR mechanism in the silica/PANI PNCs is shown in Scheme 1.

3.7. Effect of Particle Size on Properties of the Silica/PANI PNCs. In this work, the effect of particle size on the properties of the silica/PANI nanocomposites is studied. The small sized silica (20−30 nm)/PANI nanocomposites with a silica nanoparticle loading of 10.0 and 20.0 wt % were synthesized for comparison. The thermal stability of the small sized silica/PANI nanocomposites is summarized in Table 1. The TGA curves, dielectric properties, and temperature dependent resistivity are provided in the Supporting Information. The TEM images of the as-received silica nanoparticles and the synthesized small silica (20−30 nm)/PANI nanocomposites are shown in Figure 7A and B, respectively. The average size of the small silica nanoparticles is about 21.3 nm, which is consistent with the information provided by the company. A clear shell coating is observed outside the silica nanoparticles, Figure 7B, indicating the presence of the PANI layer. The electrical conduction mechanism is also evaluated by the Mott VRH approach as aforementioned eq 1, and the results are shown in Figure 7C. The obtained T_0, σ_0, and ρ_r of the synthesized small sized silica (20−30 nm)/PANI nanocomposites are summarized in Table 2. For the PANI PNCs with 10.0 wt % loading of small silica NPs, the T_0 and σ_0 are very close to those of the PANI nanocomposites with the same loading of the big silica nanoparticles and have no obvious changes. However, as the loading increases to 20.0 wt %, the T_0 and σ_0 of the silica/PANI nanocomposites with small silica nanoparticles are much lower than those of the PANI nanocomposites with the same loading of big silica nanoparticles. The ρ_r of the small silica/PANI nanocomposites is lower than that of big silica/PANI nanocomposites, indicating that less disorder is in the small silica/PANI PNC system.[56]

The room temperature MR values of the small silica/PANI nanocomposites with a loading of 10.0 and 20.0 wt %, Figure 7D, are observed to be almost the same as those of the big silica/PANI nanocomposites, indicating that the nanoparticle size has no obvious effect on the MR value. Mahesh et al.[69] have investigated the effect of particle size on the electron transport and magnetic properties of $La_{0.7}Ca_{0.3}MnO_3$ and found that the maximum MR of the samples at near T_c (ferromagnetic Curie temperature, above which a ferromagnetic material becomes paramagnetic) is not sensitive to the particle size, but the MR at 4.2 K increases with decreasing particle size, which is attributed to a substantial contribution by the grain boundaries in the polycrystalline samples. The calculated localization length ξ, density of states at the Fermi level $N(E_F)$, and R_{hop} according to eqs 8, 9 and 12 are also listed in Table 3. From Table 3, it can be concluded that even the ξ and $N(E_F)$ are different for different sizes of the silica/PANI nanocomposites with the same particle loading due to the difference of T_0, the ΔR_{hop} is almost the same, which further confirms that the MR value in these silica/PANI PNCs is mainly related to the ΔR_{hop}.

4. CONCLUSIONS

The polyaniline nanocomposites reinforced with different silica nanoparticle loading levels have been synthesized using a surface initiated polymerization method. The effects of particle size on the nanocomposite properties have been systematically investigated. The introduction of the silica nanoparticles dramatically enhances the thermal stability of PANI, and the thermal stability of the silica/PANI nanocomposites is increased with increasing silica nanoparticle loading. The SEM results indicate that the silica nanoparticles have been coated with PANI. The dielectric properties of these nanocomposites are strongly related to the silica nanoparticle loading, and the H_3PO_4 doped PANI and its nanocomposites show a positive permittivity, which is different from the PTSA doped PANI (negative permittivity). The resistivity of the silica/PANI nanocomposites is observed to increase with increasing silica nanoparticle loading. The Mott variable range hopping (VRH) model is used to evaluate the electrical conduction mechanism of these nanocomposites and reveals a quasi 3-d VRH electrical conduction mechanism. A large positive magnetoresistance (MR) is observed in the nonmagnetic H_3PO_4 doped PANI (65.6%) and its nanocomposites with 20.0 wt % silica nanoparticle loading (95.6%). The observed GMR is well explained by the wave function shrinkage model by calculating the changed localization length ξ, density of states at the Fermi level $N(E_F)$, and reduced average hopping length R_{hop}. The particle sizes can affect the thermal stability, dielectric properties, and resistivity of the silica/PANI nanocomposites but have no obvious effect on the MR properties.

■ ASSOCIATED CONTENT

Supporting Information

The microscale combustion calorimetry (MCC) results, the error bar calculation, and the properties of the silica (20−30 nm)/PANI PNCs including thermal stability, flame retardant behavior, and temperature dependent resistivity. This material is available free of charge via the Internet at http://pubs.acs.org.

■ AUTHOR INFORMATION

Corresponding Author

*E-mail: zhanhu.guo@lamar.edu (Z.G.); suying.wei@lamar.edu (S.W.). Phone: (409) 880-7654 (Z.G.); (409) 880-7976 (S.W.). Fax: (409) 880-2197 (Z.G.); (409) 880-8270 (S.W.).

Notes

The authors declare no competing financial interest.

■ ACKNOWLEDGMENTS

This project is financially supported by the National Science Foundation Nanoscale Interdisciplinary Research Team, and Materials Processing and Manufacturing (CMMI 10-30755) managed by Dr. Mary Toney. D.P.Y. acknowledges the support from the NSF under Grant No. DMR 10-05764. H.G. acknowledges the support from China Scholarship Council (CSC) program.

■ REFERENCES

(1) Cheung, W.; Chiu, P. L.; Parajuli, R. R.; Ma, Y.; Ali, S. R.; He, H. Fabrication of High Performance Conducting Polymer Nanocomposites for Biosensors and Flexible Electronics: Summary of the Multiple Roles of DNA Dispersed and Functionalized Single Walled Carbon Nanotubes. *J. Mater. Chem.* **2009**, *19*, 6465−6480.

(2) Bilotti, E.; Zhang, R.; Deng, H.; Baxendale, M.; Peijs, T. Fabrication and Property Prediction of Conductive and Strain Sensing TPU/CNT Nanocomposite Fibres. *J. Mater. Chem.* **2010**, *20*, 9449−9455.

(3) Ding, K.; Jia, H.; Wei, S.; Guo, Z. Electrocatalysis of Sandwich-Structured Pd/Polypyrrole/Pd Composites toward Formic Acid Oxidation. *Ind. Eng. Chem. Res.* **2011**, *50*, 7077−7082.
(4) Zhu, J.; Wei, S.; Zhang, L.; Mao, Y.; Ryu, J.; Mavinakuli, P.; Karki, A. B.; Young, D. P.; Guo, Z. Conductive Polypyrrole/Tungsten Oxide Metacomposites with Negative Permittivity. *J. Phys. Chem. C* **2010**, *114*, 16335−16342.
(5) Zhu, J.; Wei, S.; Alexander, M. J.; Dang, T. D.; Ho, T. C.; Guo, Z. Enhanced Electrical Switching and Electrochromic Properties of Poly(p-phenylenebenzobisthiazole) Thin Films Embedded with Nano-WO_3. *Adv. Funct. Mater.* **2010**, *20*, 3076−3084.
(6) Wei, H.; Yan, X.; Li, Y.; Wu, S.; Wang, A.; Wei, S.; Guo, Z. Hybrid Electrochromic Fluorescent Poly(DNTD)/CdSe@ZnS Composite Films. *J. Phys. Chem. C* **2012**, *116*, 4500−4510.
(7) Kolasinska, M.; Krastev, R.; Gutberlet, T.; Warszynski, P. Layer-by-Layer Deposition of Polyelectrolytes. Dipping versus Spraying. *Langmuir* **2008**, *25*, 1224−1232.
(8) Zhu, J.; Wei, S.; Chen, X.; Karki, A. B.; Rutman, D.; Young, D. P.; Guo, Z. Electrospun Polyimide Nanocomposite Fibers Reinforced with Core-Shell Fe-FeO Nanoparticles. *J. Phys. Chem. C* **2010**, *114*, 8844−8850.
(9) Wei, H.; Yan, X.; Li, Y.; Gu, H.; Wu, S.; Ding, K.; Wei, S.; Guo, Z. Electrochromic Poly(DNTD)/WO_3 Nanocomposite Films via Electropolymerization. *J. Phys. Chem. C* **2012**, *116* (30), 16286−16293.
(10) Guo, Z.; Kim, T. Y.; Lei, K.; Pereira, T.; Hahn, H. T. Strengthening and Thermal Stabilizing Polyurethane Nanocomposites with Silicon Carbide Nanoparticles through Surface-Initiated-Polymerization Approach. *Compos. Sci. Technol.* **2008**, *68*, 164−170.
(11) Zhu, J.; Gu, H.; Luo, Z.; Haldolaarachige, N.; Young, D. P.; Wei, S.; Guo, Z. Carbon Nanostructure-Derived Polyaniline Metacomposites: Electrical, Dielectric, and Giant Magnetoresistive Properties. *Langmuir* **2012**, *28*, 10246−10255.
(12) MacDiarmid, A. G. Synthetic Metals: A Novel Role for Organic Polymers (Nobel Lecture). *Angew. Chem., Int. Ed.* **2001**, *40*, 2581−2590.
(13) Huang, J.; Virji, S.; Weiller, B. H.; Kaner, R. B. Nanostructured Polyaniline Sensors. *Chem.—Eur. J.* **2004**, *10*, 1314−1319.
(14) Lu, W.; Fadeev, A. G.; Qi, B.; Smela, E.; Mattes, B. R.; Ding, J.; Spinks, G. M.; Mazurkiewicz, J.; Zhou, D.; Wallace, G. G.; et al. Use of Ionic Liquids for π-Conjugated Polymer Electrochemical Devices. *Science* **2002**, *297*, 983−987.
(15) Wei, H.; Yan, X.; Wu, S.; Luo, Z.; Wei, S.; Guo, Z. Electropolymerized Polyaniline Stabilized Tungsten Oxide Nanocomposite Films: Electrochromic Behavior and Electrochemical Energy Storage. *J. Phys Chem. C* **2012**, *116*, 25052−25064.
(16) Gómez-Romero, P.; Torres-Gómez, G. Molecular Batteries: Harnessing $Fe(CN)_6^{3-}$ Electroactivity in Hybrid Polyaniline−Hexacyanoferrate Electrodes. *Adv. Mater.* **2000**, *12*, 1454−1456.
(17) Walther, J. *Essentials of Geochemistry*; Jones & Bartlett Learning: 2009; pp 158−159.
(18) Kingon, A. I.; Maria, J.; Streiffer, S. K. Alternative Dielectrics to Silicon Dioxide for Memory and Logic Devices. *Nature* **2000**, *406*, 1032−1038.
(19) Couleaud, P.; Morosini, V.; Frochot, C.; Richeter, S.; Raehm, L.; Durand, J. Silica-Based Nanoparticles for Photodynamic Therapy Applications. *Nanoscale* **2010**, *2*, 1083−1095.
(20) Bringas, E.; Koysuren, O.; Quach, D. V.; Mahmoudi, M.; Aznar, E.; Roehling, J. D.; Marcos, M. D.; Martinez-Manez, R.; Stroeve, P. Triggered Release in Lipid Bilayer-Capped Mesoporous Silica Nanoparticles Containing SPION Using an Alternating Magnetic Field. *Chem. Commun.* **2012**, *48*, 5647−5649.
(21) Vila, M.; Hueso, J. L.; Manzano, M.; Izquierdo-Barba, I.; Andres, A.; Sanchez, J.; Prieto, C.; Vallet-Regi, M. Carbon Nanotubes-Mesoporous Silica Composites as Controllable Biomaterials. *J. Mater. Chem.* **2009**, *19*, 7745−7752.
(22) Mihalcik, D. J.; Lin, W. Mesoporous Silica Nanosphere Supported Ruthenium Catalysts for Asymmetric Hydrogenation. *Angew. Chem., Int. Ed.* **2008**, *47*, 6229−6232.
(23) Comes, M.; Marcos, M. D.; Martinez-Manez, R.; Sancenon, F.; Villaescusa, L. A.; Graefe, A.; Mohr, G. J. Hybrid Functionalised Mesoporous Silica-Polymer Composites for Enhanced Analyte Monitoring Using Optical Sensors. *J. Mater. Chem.* **2008**, *18*, 5815−5823.
(24) Zhu, J.; Wei, S.; Lee, I. Y.; Park, S.; Willis, J.; Haldolaarachchige, N.; Young, D. P.; Luo, Z.; Guo, Z. Silica Stabilized Iron Particles toward Anti-Corrosion Magnetic Polyurethane Nanocomposites. *RSC Adv.* **2012**, *2*, 1136−1143.
(25) Peng, H.; Jain, M.; Peterson, D. E.; Zhu, Y.; Jia, Q. Composite Carbon Nanotube/Silica Fibers with Improved Mechanical Strengths and Electrical Conductivities. *Small* **2008**, *4*, 1964−1967.
(26) Shim, G. H.; Han, M. G.; Sharp-Norton, J. C.; Creager, S. E.; Foulger, S. H. Inkjet-Printed Electrochromic Devices Utilizing Polyaniline-Silica and Poly(3,4-ethylenedioxythiophene)-Silica Colloidal Composite Particles. *J. Mater. Chem.* **2008**, *18*, 594−601.
(27) Niu, Z.; Yang, Z.; Hu, Z.; Lu, Y.; Han, C. C. Polyaniline−Silica Composite Conductive Capsules and Hollow Spheres. *Adv. Funct. Mater.* **2003**, *13*, 949−954.
(28) Liu, Y. D.; Fang, F. F.; Choi, H. J. Silica Nanoparticle Decorated Polyaniline Nanofiber and Its Electrorheological Response. *Soft Mater.* **2011**, *7*, 2782−2789.
(29) Baibich, M. N.; Broto, J. M.; Fert, A.; Nguyen Van Dau, F.; Petroff, F.; Etienne, P.; Creuzet, G.; Friederich, A.; Chazelas, J. Giant Magnetoresistance of (001)Fe/(001)Cr Magnetic Superlattices. *Phys. Rev. Lett.* **1988**, *61*, 2472−2475.
(30) Edelstein, R. L.; Tamanaha, C. R.; Sheehan, P. E.; Miller, M. M.; Baselt, D. R.; Whitman, L. J.; Colton, R. J. The BARC Biosensor Applied to the Detection of Biological Warfare Agents. *Biosens. Bioelectron.* **2000**, *14*, 805−813.
(31) Sanvito, S. Molecular Spintronics. *Chem. Soc. Rev.* **2011**, *40*, 3336−3355.
(32) Wang, F.; Vardeny, Z. V. Organic Spin Valves: the First Organic Spintronics Devices. *J. Mater. Chem.* **2009**, *19*, 1685−1690.
(33) Gu, H.; Huang, Y.; Zhang, X.; Wang, Q.; Zhu, J.; Shao, L.; Haldolaarachchige, N.; Young, D. P.; Wei, S.; Guo, Z. Magnetoresistive Polyaniline-Magnetite Nanocomposites with Negative Dielectrical Properties. *Polymer* **2012**, *53*, 801−809.
(34) Zhang, X.; Wei, S.; Haldolaarachchige, N.; Colorado, H. A.; Luo, Z.; Young, D. P.; Guo, Z. Magnetoresistive Conductive Polyaniline-Barium Titanate Nanocomposites with Negative Permittivity. *J. Phys. Chem. C* **2012**, *116*, 15731−15740.
(35) Zhu, J.; Wei, S.; Zhang, L.; Mao, Y.; Ryu, J.; Karki, A. B.; Young, D. P.; Guo, Z. Polyaniline-Tungsten Oxide Metacomposites with Tunable Electronic Properties. *J. Mater. Chem.* **2011**, *21*, 342−348.
(36) Zhu, J.; Wei, S.; Zhang, L.; Mao, Y.; Ryu, J.; Haldolaarachige, N.; Young, D. P.; Guo, Z. Dielectric Properties of Polyaniline-Al_2O_3 Nanocomposites Derived from Various Al_2O_3 Nanostructures. *J. Mater. Chem.* **2011**, *21*, 3952−3959.
(37) Mavinakuli, P.; Wei, S.; Wang, Q.; Karki, A. B.; Dhage, S.; Wang, Z.; Young, D. P.; Guo, Z. Polypyrrole/Silicon Carbide Nanocomposites with Tunable Electrical Conductivity. *J. Phys. Chem. C* **2010**, *114*, 3874−3882.
(38) Pillalamarri, S. K.; Blum, F. D.; Tokuhiro, A. T.; Story, J. G.; Bertino, M. F. Radiolytic Synthesis of Polyaniline Nanofibers: A New Templateless Pathway. *Chem. Mater.* **2004**, *17*, 227−229.
(39) Bau, L.; Bartova, B.; Arduini, M.; Mancin, F. Surfactant-Free Synthesis of Mesoporous and Hollow Silica Nanoparticles with an Inorganic Template. *Chem. Commun.* **2009**, 7584−7586.
(40) Xuan, S.; Wang, Y. X. J.; Leung, K. C. F.; Shu, K. Synthesis of Fe_3O_4@polyaniline Core/shell Microspheres with Well-Defined Blackberry-Like Morphology. *J. Phys. Chem. C* **2008**, *112*, 18804−18809.
(41) Guo, Z.; Shin, K.; Karki, A.; Young, D.; Kaner, R.; Hahn, H. Fabrication and Characterization of Iron Oxide Nanoparticles Filled Polypyrrole Nanocomposites. *J. Nanopart. Res.* **2009**, *11*, 1441−1452.
(42) Li, B.; Sui, G.; Zhong, W. Single Negative Metamaterials in Unstructured Polymer Nanocomposites Toward Selectable and Controllable Negative Permittivity. *Adv. Mater.* **2009**, *21*, 4176−4180.

(43) Joo, J.; Oh, E. J.; Min, G.; MacDiarmid, A. G.; Epstein, A. J. Evolution of the Conducting State of Polyaniline from Localized to Mesoscopic Metallic to Intrinsic Metallic Regimes. *Synth. Met.* **1995**, *69*, 251−254.
(44) Barut, G.; Pissis, P.; Pelster, R.; Nimtz, G. Glass Transition in Liquids: Two versus Three-Dimensional Confinement. *Phys. Rev. Lett.* **1998**, *80*, 3543−3546.
(45) Baskaran, S.; Liu, J.; Domansky, K.; Kohler, N.; Li, X.; Coyle, C.; Fryxell, G. E.; Thevuthasan, S.; Williford, R. E. Low Dielectric Constant Mesoporous Silica Films through Molecularly Templated Synthesis. *Adv. Mater.* **2000**, *12*, 291−294.
(46) Lee, K.; Cho, S.; Park, S. H.; Heeger, A. J.; Lee, C. W.; Lee, S. H. Metallic Transport in Polyaniline. *Nature* **2006**, *44*, 65−68.
(47) Adams, P. N.; Laughlin, P. J.; Monkman, A. P.; Kenwright, A. M. Low Temperature Synthesis of High Molecular Weight Polyaniline. *Polymer* **1996**, *37*, 3411−3417.
(48) Stejskal, J.; Sapurina, I.; Trchová, M.; Prokeš, J.; Křivka, I.; Tobolková, E. Solid-State Protonation and Electrical Conductivity of Polyaniline. *Macromolecules* **1998**, *31*, 2218−2222.
(49) Sproul, A. B.; Green, M. A. Improved Value for the Silicon Intrinsic Carrier Concentration from 275 to 375 K. *J. Appl. Phys.* **1991**, *70*, 846−854.
(50) Deng, J.; Ding, X.; Zhang, W.; Peng, Y.; Wang, J.; Long, X.; Li, P.; Chan, A. S. C. Magnetic and Conducting Fe_3O_4-Cross-Linked Polyaniline Nanoparticles with Core-Shell Structure. *Polymer* **2002**, *43*, 2179−2184.
(51) Zhang, X.; Zhu, J.; Haldolaarachchige, N.; Ryu, J.; Young, D. P.; Wei, S.; Guo, Z. Synthetic Process Engineered Polyaniline Nanostructures with Tunable Morphology and Physical Properties. *Polymer* **2012**, *53*, 2109−2120.
(52) Zhang, L.; Tang, Z. Polaron Relaxation and Variable-Range-Hopping Conductivity in the Giant-Dielectric-Constant Material $CaCu_3Ti_4O_{12}$. *Phys. Rev. B* **2004**, *70*, 174306.
(53) Spatz, J. P.; Lorenz, B.; Weishaupt, K.; Hochheimer, H. D.; Menon, V.; Parthasarathy, R.; Martin, C. R.; Bechtold, J.; Hor, P. Observation of Crossover from Three- to Two-Dimensional Variable-Range Hopping in Template-Synthesized Polypyrrole and Polyaniline. *Phys. Rev. B* **1994**, *50*, 14888−14892.
(54) Dietrich, C. P.; Lange, M.; Benndorf, G.; Lenzner, J.; Lorenz, M.; Grundmann, M. Competing Exciton Localization Effects due to Disorder and Shallow Defects in Semiconductor Alloys. *New J. Phys.* **2010**, *12*, 033030.
(55) Galvo, D.; Dos Santos, D.; Laks, B.; Melo, C. de; Caldas, M. Role of Disorder in the Conduction Mechanism in Polyanilines. *Phys. Rev. Lett.* **1989**, *63*, 786−789.
(56) Sarkar, A.; Ghosh, P.; Meikap, A. K.; Chattopadhyay, S. K.; Chatterjee, S. K.; Ghosh, M. Direct and Alternate Current Conductivity and Magnetoconductivity of Oxalic Acid Doped Polyaniline. *Solid State Commun.* **2007**, *143*, 358−363.
(57) Gupta, K.; Jana, P. C.; Meikap, A. K. Electrical Transport and Optical Properties of the Composite of Polyaniline Nanorod with Gold. *Solid State Sci.* **2012**, *14*, 324−329.
(58) Gangopadhyay, R.; De, A.; Das, S. Transport Properties of Polypyrrole-Ferric Oxide Conducting Nanocomposites. *J. Appl. Phys.* **2000**, *87*, 2363−2367.
(59) Lordi, V.; Erhart, P.; Åberg, D. Charge Carrier Scattering by Defects in Semiconductors. *Phys. Rev. B* **2010**, *81*, 235204.
(60) Sodha, M. S.; Arora, A. K.; Kaw, P. K. Amplitude Modulation of Electromagnetic Waves by Alternating Magnetic Fields. *J. Phys. A: Gen. Phys.* **1968**, *1*, 89−96.
(61) Guo, Z.; Moldovan, M.; Young, D. P.; Henry, L. L.; Podlaha, E. J. Magnetoresistance and Annealing Behaviors of Particulate Co-Au Nanocomposites. *Electrochem. Solid-State Lett.* **2007**, *10*, E31−E35.
(62) Mermer, Ö.; Veeraraghavan, G.; Francis, T. L.; Sheng, Y.; Nguyen, D. T.; Wohlgenannt, M.; Köhler, A.; Al-Suti, M. K.; Khan, M. S. Large Magnetoresistance in Nonmagnetic π-Conjugated Semiconductor Thin Film Devices. *Phys. Rev. B* **2005**, *72*, 205202.
(63) Su, T.; Wang, C.; Lin, S.; Rosenbaum, R. Magnetoresistance of $Al_{70}Pd_{22.5}Re_{7.5}$ Quasicrystals in the Variable-Range Hopping Regime. *Phys. Rev. B* **2002**, *66*, 054438.
(64) Shklovskii, B. I.; ShklovskiÄ, B. I.; Ėfros, A. L. *Electronic Properties of Doped Semiconductors*; Springer-Verlag: 1984; Appdex 3.
(65) Dutta, K.; De, S. K. Optical and Electrical Characterization of Polyaniline-silicon Dioxide Nanocomposite. *Phys. Rev. A* **2007**, *361*, 141−145.
(66) Entin-Wohlman, O.; Imry, Y.; Sivan, U. Orbital Magneto-conductance in the Variable-Range-Hopping Regime. *Phys. Rev. B* **1989**, *40*, 8342−8348.
(67) Sivan, U.; Entin-Wohlman, O.; Imry, Y. Orbital Magneto-conductance in the Variable-Range-Hopping Regime. *Phys. Rev. Lett.* **1988**, *60*, 1566−1569.
(68) Zhang, Y.; Sarachik, M. P. Negative Magnetoresistance in the Variable-Range-Hopping Regime in n-Type CdSe. *Phys. Rev. B* **1991**, *43*, 7212−7215.
(69) Mahesh, R.; Mahendiran, R.; Raychaudhuri, A. K.; Rao, C. N. R. Effect of Particle Size on the Giant Magnetoresistance of $La_{0.7}Ca_{0.3}MnO_3$. *Appl. Phys. Lett.* **1996**, *68*, 2291−2293.